Biomedicine & Pharmacotherapy 174 (2024) 116441

Contents lists available at ScienceDirect

Biomedicine & Pharmacotherapy

journal homepage: www.elsevier.com/locate/biopha

Intranasal administration of *Escherichia coli Nissle* expressing the spike protein of SARS-CoV-2 induces long-term immunization and prevents spike protein-mediated lung injury in mice

Giovanni Sarnelli [a,b,1], Alessandro Del Re [c,1], Irene Palenca [c,1], Silvia Basili Franzin [c], Jie Lu [b,d], Luisa Seguella [c,*], Aurora Zilli [c], Marcella Pesce [a], Sara Rurgo [a], Giovanni Esposito [b,e], Walter Sanseverino [b], Giuseppe Esposito [b,c]

[a] Department of Clinical Medicine and Surgery, Section of Gastroenterology, University Federico II, Naples 80138, Italy
[b] Nextbiomics S.R.L. (Società a Responsabilità Limitata), Naples 80100, Italy
[c] Department of Physiology and Pharmacology "V. Erspamer", Sapienza University of Rome, Rome 00185, Italy
[d] Department of Anatomy and Cell Biology, China Medical University, Shenyang 110122, China
[e] Department of Molecular Medicine and Medical Biotechnologies, Centro Ingegneria Genetica-Biotecnologie Avanzate s.c.a rl, Naples 80131, Italy

ARTICLE INFO

Keywords:
COVID-19
Engineered probiotics
IgA
NLRP3
Intranasal vaccine
Mice lung injury
Spike protein

ABSTRACT

While current anti-Spike protein (SP) vaccines have been pivotal in managing the pandemic, their limitations in delivery, storage, and the inability to provide mucosal immunization (preventing infections) highlight the ongoing necessity for research and innovation. To tackle these constraints, our research group developed a bacterial-based vaccine using a non-pathogenic *E. coli Nissle 1917* (EcN) strain genetically modified to express the SARS-CoV-2 spike protein on its surface (EcN-pAIDA1-SP). We intranasally delivered the EcN-pAIDA1-SP in two doses and checked specific IgG/IgA production as well as the key immune mediators involved in the process. Moreover, following the initial and booster vaccine doses, we exposed both immunized and non-immunized mice to intranasal delivery of SARS-CoV-2 SP to assess the effectiveness of EcN-pAIDA1-SP in protecting lung tissue from the inflammation damage. We observed detectable levels of anti-SARS-CoV-2 spike IgG in serum samples and IgA in bronchoalveolar lavage fluid two weeks after the initial treatment, with peak concentrations in the respective samples on the 35th day. Moreover, immunoglobulins displayed a progressively enhanced avidity index, suggesting a selective binding to the spike protein. Finally, the pre-immunized group displayed a decrease in proinflammatory markers (TLR4, NLRP3, ILs) following SP challenge, compared to the non-immunized groups, along with better preservation of tissue morphology. Our probiotic-based technology provides an effective immunobiotic tool to protect individuals against disease and control infection spread.

1. Introduction

Over the past four years, the global community has confronted the profound ramifications of the COVID-19 pandemic, extending beyond immediate health concerns to encompass significant economic and social challenges. The rapid global spread of SARS-CoV-2 in our interconnected and globalized societies prompted the World Health Organization to state COVID-19 a pandemic by March 11, 2020. Although the pandemic phase of COVID 19 infection has been declared concluded on May 5th 2023 by the WHO, on February 4, 2024, over 774 million confirmed cases and more than seven million deaths have been reported globally (https://covid19.who.int/).

The urgent need for a more effective and fast response from the global scientific and healthcare communities is a still significant challenge.

The etiopathogenic agent of COVID-19 is SARS-CoV-2, which

* Corresponding author.
E-mail addresses: sarnelli@unina.it (G. Sarnelli), alessandro.delre@uniroma1.it (A. Del Re), irene.palenca@uniroma1.it (I. Palenca), silvia.basilifranzin@uniroma1.it (S.B. Franzin), lvjie@cmu.edu.cn (J. Lu), luisa.seguella@uniroma1.it (L. Seguella), aurora.zilli@uniroma1.it (A. Zilli), sara.rurgo@unina.it (S. Rurgo), espogiov@unina.it (G. Esposito), wsanseverino@sequentiabiotech.com (W. Sanseverino), giuseppe.esposito@uniroma1.it (G. Esposito).
[1] These authors equally contributed to this work.

https://doi.org/10.1016/j.biopha.2024.116441
Received 23 February 2024; Received in revised form 13 March 2024; Accepted 15 March 2024
Available online 21 March 2024

belongs to the *Coronaviridae* family and infects human cells by directly interacting with the angiotensin-converting enzyme-2 (ACE-2) through the viral Spike Protein (SP) [1]. Consequently, the SP is the targeted antigen for vaccine development [2–4].

While current anti-SP vaccines have been pivotal in managing the pandemic, their limitations in delivery, storage, and the inability to provide mucosal immunization (preventing infections) highlight the ongoing necessity for research and innovation. This is vital not only for addressing existing challenges but also for preparing against future pandemics [5–7].

To tackle these constraints, our research group developed a bacterial-based vaccine using a non-pathogenic *E. coli Nissle 1917* (EcN) strain genetically modified to express the SARS-CoV-2 SP on its surface (EcN-pAIDA1-SP), leveraging the bacteria's immunogenicity [8]. Specifically, we engineered an EcN strain with a plasmid encoding SP, utilizing the adhesin involved in diffuse adherence 1 (AIDA1) as an autotransporter (pAIDA1-SP). This design facilitates the surface expression of SARS-CoV-2 SP on the otherwise non-pathogenic bacteria. The presentation of the viral epitope by commensal bacteria not only extends its half-life upon administration but also enhances the immune response, as the surface proteins of gram-negative bacteria serve as adjuvants [9,10].

Several bacteria have been investigated as delivery systems to express recombinant proteins. For example, *E. coli* represents one of the most studied and employed microorganisms due to its safety profile, high growth rate, genomic simplicity, and ease of handling [11–13]. A proof-of-concept study introduced a killed whole-genome-reduced E. coli vaccine with a surface expression of the SARS-CoV-2 fusion peptide, and the authors reported the feasibility of this platform against SARS-CoV-2. Although promising, this approach failed to elicit strong neutralizing humoral immune responses against the fusion peptides in a porcine model [14].

Preliminary evaluations demonstrated the effectiveness of EcN-pAIDA1-SP in eliciting long-term systemic IgG-mediated immunization against SP following oral administration, coupled with a strong mucosal IgA response [15]. This is particularly noteworthy considering that only a limited number of currently available vaccines have been assessed for their ability to induce mucosal protection in both the upper (URT) and lower respiratory tract (LRT) [16,17]. Indeed, the nasal turbinate (NT) in the URT stands out as one of the most critical entry points for SARS-CoV-2 in humans. Ciliated nasal epithelial cells in the NT exhibit the highest expression of ACE2 and transmembrane serine protease 2 (TMPRSS2) [18] — another crucial receptor for SARS-CoV-2 entry and infection. Additionally, the LRT tissue also expresses a significant amount of ACE2 in various cell types, including macrophages, bronchial and tracheal epithelial cells, and type 2 pneumocytes [19], making the LRT another crucial area for SARS-CoV-2 infection. The revelation that EcN-pAIDA1-SP can induce a targeted mucosal IgA-mediated response in the lungs instills confidence in its potential as a promising strategy for preventing viral spread [20,21].

While the currently available vaccines may not entirely prevent infection, they notably provide robust protection against severe clinical outcomes, such as acute respiratory distress syndrome (ARDS) and multiorgan failure associated with the advanced stages of the disease [4]. ARDS occurs when macrophages and mast cells fail to regulate the innate immune response [22,23], leading to an excessive release of pro-inflammatory mediators [24,25], which is further amplified by the activation of the NOD-like receptor family pyrin domain containing 3 (NLRP3) inflammasome [26,27].

It appears that the SP of SARS-CoV-2 initiates a hyper-inflammatory response through its interaction with Toll-like receptor 4 (TLR4) [28]. Substantial research from our group and others has established a direct association between these components, playing a pivotal role in the development of ARDS and various short-term and long-term manifestations of COVID-19 [29,30]. In a prior publication, we proposed a potential mechanism by which the interaction of SP with TLR4 induces this inflammatory milieu, involving the phospho-p38/NF-κB/NLRP3 pathway [31]. Additionally, we demonstrated the up-regulation of ACE-2 receptor expression in different cell subtypes during SP-induced inflammatory conditions, possibly linked to TLR4-related downstream products [32].

Based upon these notions, an anti-SARS-CoV-2 vaccine able to trigger the production of mucosal IgA against SP may operate on a dual level: opsonization of viral particles preventing the infection and direct interference with SP-TLR4 interaction to mitigate the pro-inflammatory action of this antigen [33].

In this research paper, we assessed the capability of EcN-pAIDA1-SP to induce specific IgG/IgA-mediated long-term immunization against the SARS-CoV-2 SP through intranasal delivery of the engineered bacteria. Additionally, we examined the main immune mediators involved in the process. Moreover, following the initial and booster vaccine doses, we exposed both immunized and non-immunized mice to intranasal delivery of SARS-CoV-2 SP to assess the efficacy of EcN-pAIDA1-SP in protecting lung tissue from the pro-inflammatory environment.

2. Materials and methods

2.1. Generation of E. coli Nissle expressing SARS-CoV-2 spike protein on the cell membrane as an immunogen

The adhesin involved in diffuse adherence (AIDA) of *E. coli* has been used for the expression of recombinant proteins on the outer membrane of E. coli. The surface translocation system of AIDA-I is an anchor protein from the *Escherichia coli (Escherichia coli strain 2787)*. Surface expression using AIDA required three parts: signal peptide, passenger domain, and anchor protein AIDAc. The signal peptide aided in transporting the protein to the membrane, the passenger domain was the protein of interest, and the AIDAc was the anchor protein, whose β-barrel structure could be anchored on the outer membrane so that the protein of interest could be expressed on the surface. A specific plasmid pAIDA1 was exploited to express the SARS-CoV-2 SP on the EcN membrane.

The plasmid coding for the SARS-CoV-2 SP was purchased from Genewiz, Suzhou, China, product cat n° GS-200519_A001 (https://climsprod.genewiz.com.cn/ECProduct/Products/S-in-pCDNA3-1, accessed on 3 February 2022), and we cloned the SARS-CoV-2 SP from this plasmid for the pAIDA1 vector. The primers for RT-PCR are listed below (the red sequences are flanking sequences around the *Kpn*I/*Sac*I sites from the pAIDA1 vector (Addgene 79180, http://www.addgene.org/79180/, accessed on 3 February 2022), which were used for overlapping in-fusion in the next step:

Spike-FW2:
CAGGGTCCGGGTACCATGTTTGTTTTTCTTGTTTTATTGC

Spike-RV2: CAGGTTTTCGAGCTCTGTGTAATGTAATTTGACTCC

The pAIDA1 vector was digested with *Kpn*I/*Sac*I, and the PCR product was inserted into the cutting site by using the in-fusion method from Clontech, resulting in the pAIDA1-SP. The plasmid was transduced into the EcN and confirmed by Western blotting and immunofluorescent microscopy for the expression of the spike protein on the outer membrane of the EcN [15].

2.2. Animals, immunization protocol, and sample collection

All experiments involving animals were conductedaccording to the Federico II University's Ethics Committee (Organizzazione per il benessere animale, OPBA). All animal experiments complied with the ARRIVE guidelines and were carried out following the U.K. Animals (Scientific Procedures) Act, 1986, and associated guidelines, E.U. Directive 2010/63/EU for animal experiments. Six-week-old female C57BL/6Jmice were used for the experiments (Charles River, Lecco, Italy). All mice were maintained on a 12 h light/dark cycle in a temperature-controlled environment with access to food and water *ad libitum*. The mice were euthanized at various time points by CO_2-induced

hypoxia. We conducted an initial set of experiments to assess the safety of the intranasally administered probiotic EcN-pAIDA1-SP at days 14 and 35 and its ability to elicit a consistent immunological memory following the booster dos at day 28. In the second set of experiments, we investigated whether the treatment with EcN-pAIDA1-SP effectively prevents lung damage and the upregulation of pro-inflammatory markers that follow the intranasal administration SARS-CoV-2-SP in both the acute (post-intranasal administration of SP 50 ng/mouse) and chronic (25 days post-intranasal administration of SP 50 ng/mouse) phases of the disease. Here, mice were randomly divided into 5 groups of 12 animals each: (1) Vehicle; (2) SP; (3) EcN-pAIDA1-SP; (4) EcN-pAIDA1-SP + SP; (5) EcN-pAIDA1 + SP. The entire protocol lasted 60 days, and the 5 groups received treatments listed in Table 1.

For the intranasal administration, volumes (10 μl each) of bacterial suspensions, SP solution or vehicle were intranasally delivered dropwise to the nares using a pipetman (model P20, Gilson) while the mouse was in a supine position. A total of N = 4 animals were euthanized on days 14, 35, 42, and 60 (Scheme 1).

2.3. Sample collection and preparation

Blood samples were collected from the tail vein [34] at each time point. Blood samples were stored at 37 °C for 1 h, and then the serum was separated from blood cells by centrifuging at 12,000 RPM for 5 min [35]. Serum samples were stored at −80 °C until they were analyzed.

Broncho-alveolar lavage fluid (BALF) was collected follows. Mice were dissected to expose the trachea, and a small incision was made. A sterile tube (diameter 0.58 mm) was inserted through the incision and connected to a sterile syringe needle. To create an airtight seal, a piece of sterile surgical thread was tightly wrapped around the intubated trachea. Two rounds of instillation and retrieval of 1 mL of sterile phosphate-buffered saline (PBS) into the lungs were then performed using the sterile syringe. To ensure the integrity of the procedure, the tubing-needle-syringe setup was rinsed thoroughly with sterile PBS between each sample collection. Sterile PBS (n=2) was used for lavage, and PBS rinses (n=4) of the syringe, needle, and tubing (before and after lavage) were collected as procedural controls. BALF was prepared by pooling the two sequential lavages from each mouse, resulting in up to 2 mL of total BALF per mouse.

To prepare perfused lungs for H&E and immunofluorescence analysis, a solution of 4% PFA was injected directly into the lung through the trachea, which was then secured with a piece of thread. The lungs were subsequently immersed in the same fixative for 24 h. Following fixation, the lungs were perfused and then immersed in 30% sucrose for 24 h.

Table 1
Experimental groups and treatments along the 60 days of the experimental plan.

Groups	Days 0–3 (1st dose)	Day 21 (Booster dose)	Days 35–42
(1) Vehicle	Intranostril delivery of sterile PBS	Intranostril delivery of sterile PBS	Intranostril delivery of sterile PBS
(2) SP	Intranostril delivery of sterile PBS	Intranostril delivery of sterile PBS	Intranostril delivery of Spike protein (50 ng/mouse) in sterile PBS
(3) EcN-pAIDA1-SP	Intranostril delivery of EcN-pAIDA1-SP (10^9 CFU)	Intranostril delivery of EcN-pAIDA1-SP (10^9 CFU)	Intranostril delivery of sterile PBS
(4) EcN-pAIDA1-SP + SP	Intranostril delivery of EcN-pAIDA1-SP (10^9 CFU)	Intranostril delivery of EcN-pAIDA1-SP (10^9 CFU)	Intranostril delivery of Spike protein (50 ng/mouse) in sterile PBS
(5) EcN-pAIDA1 + SP	Intranostril delivery of EcN-pAIDA1 (10^9 CFU)	Intranostril delivery of EcN-pAIDA1 (10^9 CFU)	Intranostril delivery of Spike protein (50 ng/mouse) in sterile PBS

Lung's homogenates were obtained from non-PFA fixed lungs. The snap-frozen lungs were thawed, weighed, transferred to different tubes on ice containing hypotonic lysis buffer (10 mM 4-(2-hydroxyethyl)-1-piperazineethanesulfonic acid (HEPES), 1.5 mM $MgCl_2$, 10 mM KCl, 0.5 mM phenylmethylsulphonylfluoride, 1.5 mg/mL soybean trypsin inhibitor, 7 mg/mL pepstatin A, 5 mg/mL leupeptin, 0.1 mM benzamidine and 0.5 mM dithiothreitol (DTT)). The samples were centrifuged at 10,000 RPM for 10 min and supernatants were transferred to clean microcentrifuge tubes, frozen on dry ice and stored at −80 °C for the analysis.

2.4. Rectal temperature assessment

Rectal temperature was measured daily for the entire duration of the experiment. To obtain the rectal temperature, the mice were hand-restrained and placed on a horizontal surface. The tail was then lifted, and the probe (covered with Vaseline) was gently inserted into the rectum, up to a fixed depth [36].

2.5. ELISA for specific anti-SARS-CoV-2 SP IgG and IgA antibodies, LPS, TNF-α and IL-1β detection

Specific anti-SARS-CoV-2-S protein IgG quantification was performed on the sera samples collected every 2 weeks (0, 2, 4, 6, 8, 10, 12, 14, and 16), using Mouse Anti-2019 nCoV(S)IgG ELISA Kit 96 T. Specific anti-SARS-CoV-2-S protein IgA levels in the BALF samples were assessed every 4 weeks (0, 4, 8, 12, and 16) using Mouse Anti-2019 nCoV(S)IgA ELISA Kit 96 T. All the ELISA analyses were performed according to the manufacturer's instructions (Fine Biotech Co., Wuhan, China). ELISA for LPS, TNF-α, and IL-1β (all from Thermo Fisher Scientific, MA, USA) was carried out on mouse plasma and homogenized lung tissue according to the manufacturer's protocol. Absorbance was measured on a microtiter plate reader. LPS levels were determined using standard curve methods.

2.6. Relative avidity index for anti-SARS-CoV-2 SP IgA and IgG

Plasma and BALF samples were tested for antibody avidity by a Mouse Anti-2019 nCoV(S)IgA and Anti-2019 nCoV(S)IgG ELISA kit equipped with recombinant SARS-CoV-2 2019 SP pre-coated wells (Fine Biotech Co., Wuhan, China). To determine the relative avidity index (RAI), two microplate wells were used for each analysis. In one well, the anti-SARS-CoV-2 ELISA was carried out according to the manufacturer's instructions while an additional urea treatment (5.5 M for 10 min) was performed in the other well to detach the low-avidity antibodies from the antigen [37–39]. The RAI was calculated as the *ratio* of the absorbance with and without urea incubation and expressed as a percentage and fold increase vs. Vehicle group.

2.7. Western blot analysis for spike protein detection in homogenized lungs tissue

40 μg of extracted proteins were electrophoretically transferred onto polyvinylidene difluoride membranes. Subsequently, the membranes were blocked with PBS containing 5% *w/v* non-fat milk powder (Sigma-Aldrich Corporation-Merk KGaA, St. Louis, MO, USA) and then incubated with rabbit SARS-CoV-2 SP S1 polyclonal antibody (1:1000 dil. *v/v*) (Invitrogen, Waltham, MA, USA). Membranes were then incubated with the specific secondary antibodies conjugated to HRP. Immune complexes were exposed to enhanced chemiluminescence detection reagents, and the blots were analyzed by scanning densitometry (Versadoc MP4000; Bio-Rad, Segrate, Italy). Results were expressed as optical density (OD; arbitrary units = mm^2).

2.8. Hematoxylin and Eosin (H&E) staining and lung injury assessment

Lungs were cryo-sectioned at 8 μm and placed onto slides. The

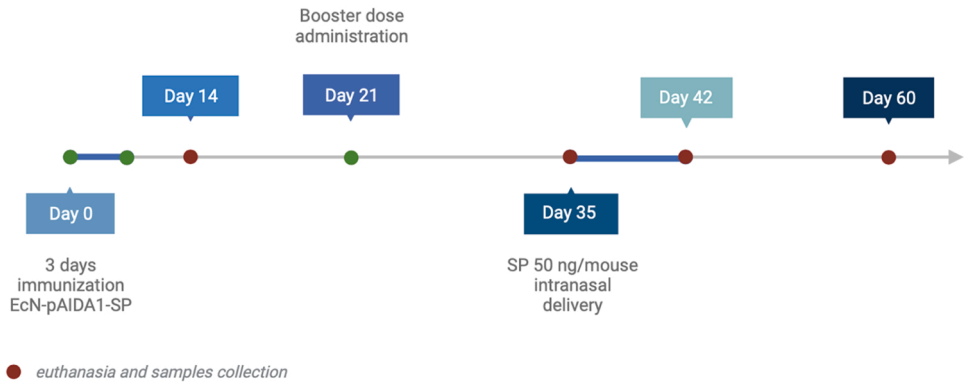

Scheme 1. Experimental time course.

sections were stained with H&E according to Ling et al. [40].The histopathological analysis has been performed in the following manner. The number of epithelial cells and the number of infiltrated neutrophils in alveolar spaces and interstitial space were analyzed by NIH Image J. 40x fields (n=10) from each group were chosen for the counting of the epithelial and infiltrated neutrophils. Lung injury score (LIS) was measured as described by Matute-Bello et al. [41,42] following a scale (Table 2).

2.9. Immunofluorescence analysis

Lungs were cryo-sectioned at 8 μm and placed onto slides. Sections were blocked with bovine serum albumin (BSA) and subsequently stained with the appropriate primary antibody (Table 3). Slices were then washed with PBS 1X and incubated in the dark with fluorescein isothiocyanate-conjugated anti-rabbit or anti-mouse (Abcam, Cambridge, UK). Nuclei were stained with Hoechst (DAPI). Sections were analyzed with a microscope (Nikon Eclipse 80i), and images were captured by a high-resolution digital camera (Nikon Digital Sight DS-U1).

2.10. Myeloperoxidase assay

Myeloperoxidase (MPO), a marker of polymorphonuclear leukocyte accumulation, was determined as previously described by Mullane et al. [43]. After removal, lung tissues were rinsed with a cold saline solution. Then, the tissues were homogenized in a solution containing 0.5% hexadecyltrimethylammonium bromide (Sigma-Aldrich, Milan, Italy), dissolved in 10 mM potassium phosphate buffer, and centrifuged for 30 min at 20,000 RPM at 37°C. An aliquot of the supernatant was mixed with a solution of tetramethylbenzidine (1.6 mM; Sigma-Aldrich, Milan, Italy) and 0.1 mM hydrogen peroxide (Sigma-Aldrich, Milan, Italy). The solution was then spectrophotometrically measured at 650 nm. MPO activity was determined as the amount of enzyme degrading 1 mmol/min of peroxide at 37°C and was expressed in milliunits (mu) per 100 mg of wet tissue weight.

Table 2
Parameters for lung injury score assessment.

Parameter		Score per field		
		0	1	2
A	Neutrophils in the alveolar space	None	1–5	> 5
B	Neutrophils in the interstitial space	None	1–5	> 5
C	Hyaline membranes	None	1	> 1
D	Proteinaceous debris filling the airspace	None	1	> 1
E	Alveolar Septal thickening	< 2X	^{2}X–^{4}X	> 4X

$$\textit{Lung injury score} = \frac{[(20*A)+(14*B)+(7*C)+(7*D)+2*E)]}{\textit{number of field}*100}$$

Table 3
Antibodies for immunofluorescence analysis.

CD-103	mouse	1:100 *v/v*	Proteintech, Manchester, UK
CD-138	mouse	1:100 *v/v*	Novus Biologicals, Abingdon, UK
TLR-4	rabbit	1:150 *v/v*	Bioss Antibodies, Boston, MA, USA
NLRP3	rabbit	1:1000 *v/v*	Invitrogen, Thermo Fisher, Waltham, MA, USA
CD-68	rabbit	1:100 *v/v*	Bioss Antibodies, Boston, MA, USA
ACE-2	mouse	1:200 *v/v*	Santa Cruz Biotechnology, Santa Cruz, CA, United States

2.11. BALF cell count

BALF was obtained from mice at each designated time point and subsequently centrifuged at 2000 RPM for 15 min. The resulting pellet was then reconstituted in 50 μl of DMEM, and an equal volume of 0.4% Trypan Blue was added and gently mixed. The mixture was incubated at room temperature (15°C – 25°C) for 5 minutes.

Subsequently, 10 μl of the stained cell suspension was carefully placed into the hemocytometer chamber. Using a hand tally counter, the cells (stained nuclei) were enumerated within each of the four external squares of the hemocytometer. The overall number of nucleated cells per milliliter was dertermined as the average cell count per square x dilution factor x 10^4 [44].

2.12. Statistical analysis

Results are expressed as the mean ± standard deviation (SD) of n experiments performed in triplicate, depending upon the experiment (see figure legends). Statistical analyses were performed using one-way ANOVA, and multiple comparisons were performed using a Bonferroni post hoc test.

3. Results

3.1. Intranasal administration of EcN-pAIDA1-SP is an effective and safe system that efficiently expresses SARS-CoV-2 spike protein without inducing lung toxicity

EcN-pAIDA1-SP did not adversely affect pulmonary physiology following both the initial and booster doses administration, as it is confirmed by histological lung injury score assessments on days 14 (Fig. 1A–B) and 35 (Fig. 1A–B). We performed ELISA tests on lung tissue homogenate to assess the levels of lipopolysaccharide (LPS), and no bacterial infections were found (Fig. 1C). Furthermore, cell count of pro-inflammatory cells in the bronchoalveolar lavage fluids (BALF) revealed no significant variations in the infiltrating cell number at pulmonary site

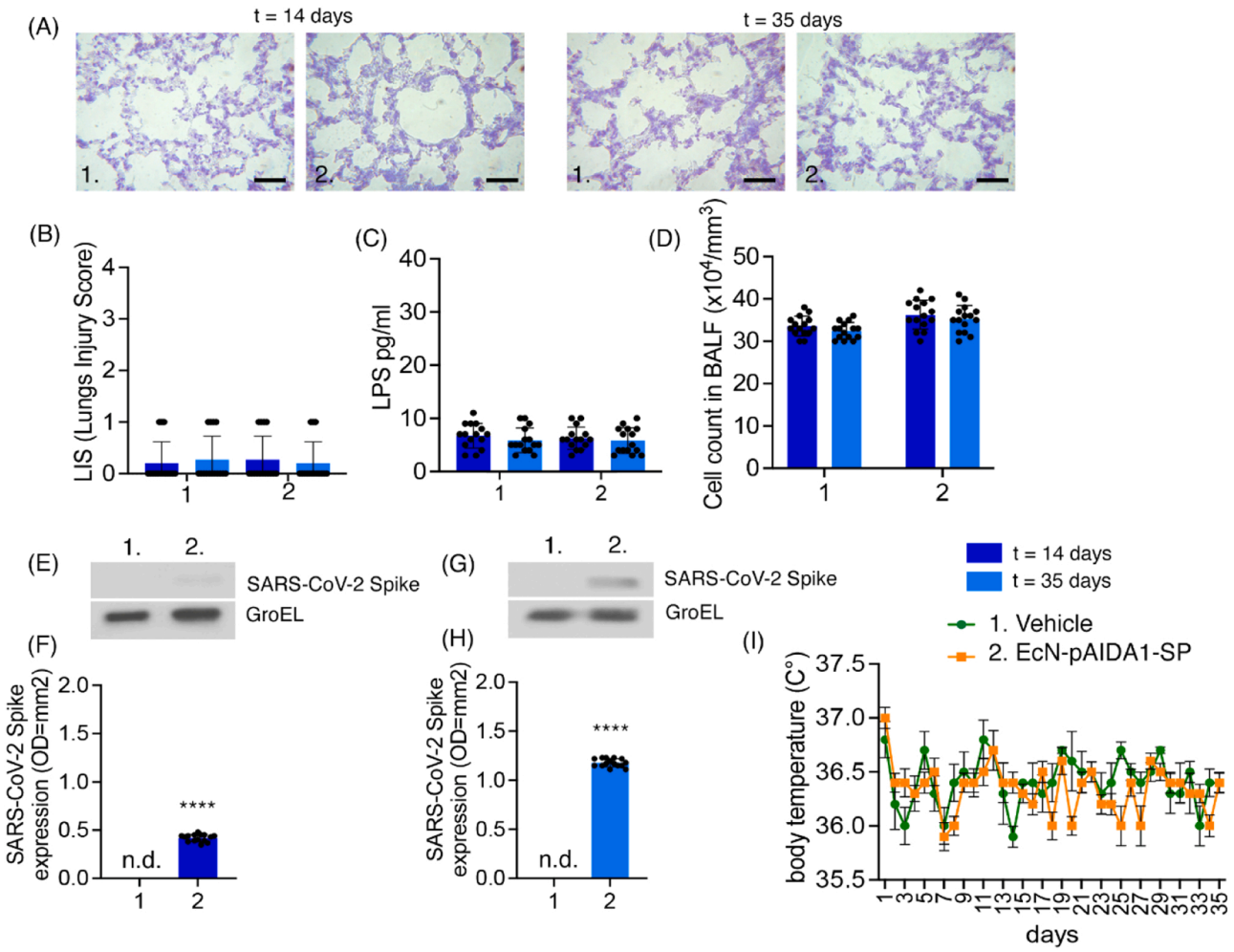

Fig. 1. EcN-pAIDA1-SP is a safe system that expresses SARS-CoV-2 spike protein. **(A)** H&E histological staining at days 14 and 35 and related **(B)** quantification of histological lung damage. **(C)** Lung endotoxemia and **(D)** cell count in bronchoalveolar fluid. Quantification of SP expression in lung tissue homogenized at days 14 **(E-F)** and 35 **(G-H)**. **(I)** Measurement of daily body temperature after intranasal probiotic administration. Results are expressed as the mean ± SD of n = 5 experiments, **** $p < 0.0001$ vs. vehicle. Image magnification 20X.

compared to the vehicle group (Fig. 1D). Then, we measured the SP levels in the lung tissue to assess the ability of EcN-pAIDA1-SP to vehicle this protein to the target tissue. The WB analysis revealed and increased expression of SARS-CoV-2 SP in the lungs of EcN-pAIDA1-SP-treated animals at both days 14 (Fig. 1E–F, 0,4193 ± 0,0367, $p < 0,0001$ **** *vs.* Vehicle) and 35 (Figs. 1I, 1,178 ± 0,0419, $p < 0,0001$ **** *vs.* Vehicle). The absence of significant variations in the body temperature of mice underwent probiotic treatment along the entire follow-up compared to the vehicle group, confirming that no pyrogenic potential is associated with the intranasal administration of EcN-pAIDA1-SP. These results demonstrate the EcN-pAIDA1-SP efficiently expresses SARS-CoV-2 spike protein and its intranasal administration represents a safe to vehicle this protein to the lung tissue.

3.2. *Engineered EcN-pAIDA1-SP elicits a time-dependent increase in adaptative immune response*

The intranasal administration of EcN-pAIDA1-SP resulted in an increase in CD138-positive cells in the lung (Figs. 2A–B, 32,73 ± 1,71, $p <$ 0,0001 **** *vs.* Vehicle at day 35) and spleen (Figs. 2A–C, 23,40 ± 2261 $p < 0,0001$ **** vs. Vehicle at day 35) compared with vehicle group, following the second boost of immunization ($p < 0,0001$ °°°° *vs. EcN-pAIDA1-SP* at day 14 for both lung and spleen). This was associated with a time-dependent rise in the anti-SARS-CoV-2 SP Immunoglobulin A (IgA) levels in the BALF (Fig. 2D, 0,0532 ± 0,0037, $p < 0,0001$ **** for day 28 *vs.* day 7; 0,0791 ± 0,0025, $p < 0,0001$ **** for day 35 *vs.* day 7) and anti- SARS-CoV-2 SP Immunoglobulin G (IgG) in the serum (Fig. 2E, 0,0779 ± 0,0089, $p < 0001$ *** for day 28 *vs.* day 7; 0,1986 ± 0,0229, $p < 0,0001$ **** for day 35 *vs.* day 7) that follow the booster dose. The progressive increase in the relative avidity index (RAI) of BALF IgA (Fig. 2F, 32,07 ± 2314, $p < 0,0001$ **** for day 28 *vs.* day 14; 40,20 ± 2145, $p < 0,0001$ **** for day 35 *vs.* day 14) and serum IgG (Fig. 2G, 21,27 ± 2052 for day 28 and 28,93 ± 2815 for day 35, $p < 0,0001$ **** *vs.* day 14), suggesting their progressive increased affinity for the viral antigen over time. Taken together, our results confirm that intranasal administration of EcN-pAIDA1-SP efficiently evokes an adaptative immune response against SARS-CoV-2 SP consequent to the boost dose administration.

3.3. *The engineered EcN-pAIDA1-SP prevents the onset of both acute and chronic lung damage and immune cells infiltration induced by SARS-CoV-2 SP*

Intranasal administration of SARS-CoV-2 SP impaired the lung tissue morphology with a significant increase of lung injury score both in acute and chronic phase of inflammation (Fig. 3A–B, 0,0957 ± 0009 $p <$ 0,0001**** for day 42 *vs.* Vehicle; 0,0448 ± 0005 $p < 0,0001$**** for day 60 *vs.* Vehicle). A parallel significant increase in pro-inflammatory

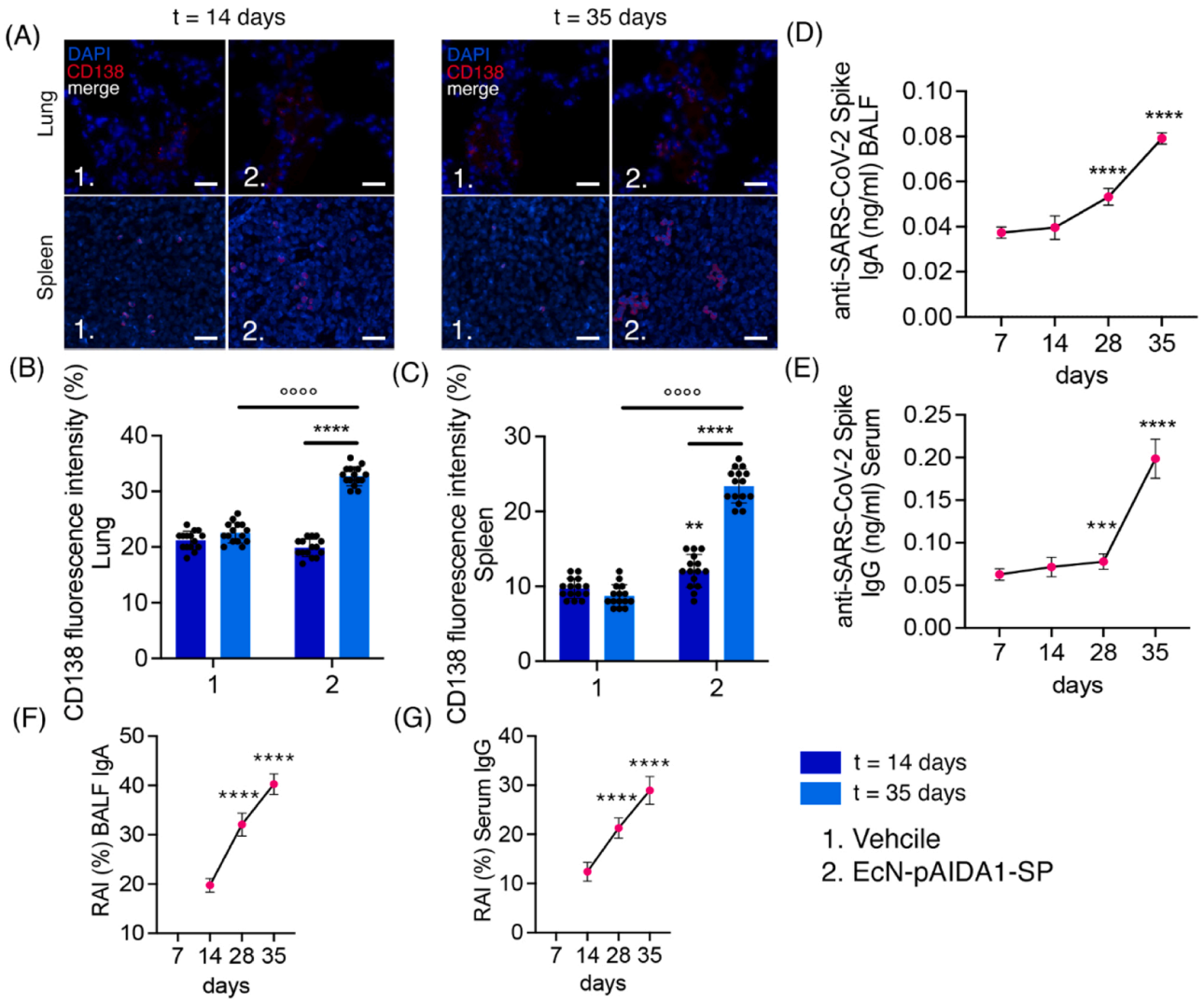

Fig. 2. EcN-pAIDA1-SP induces an IgG- and IgA-mediated response in both the lung and spleen. The images show the CD138 expression in the lungs **(A-B)** and spleen **(A-C)** at days 14 and 35, respectively. **(D)** Quantification of IgA in bronchoalveolar lavage, **(E)** IgG levels in serum, and the corresponding avidity index for IgA **(F)** and IgG **(G)**. Results are presented as the mean ± SD of n = 5 experiments **** $p < 0.0001$ and *** $p < 0.001$ vs. vehicle at day 35; °°°° $p < 0.0001$ vs. EcN-pAIDA1 at day 14. Image magnification 20X.

cells in the BALF was observed in the SP-treated mice both time points (Fig. 3C, 93,60 ± 7288, $p < 0,0001$**** for day 42 *vs.* Vehicle; 76,33 ± 6,51, $p < 0,0001$**** for day 60 *vs.* Vehicle) compared with vehicle group. The treatment with EcN-pAIDA1-SP via intranasal route prevented the histological lung damage induced by SARS-CoV-2 SP, as it was reflected by attenuated lung injury score (LIS) (Fig. 3A–B, 0,0169 ± 0,0086, $p < 0,0001$°°°° for day 42 *vs.* SP; 0,0154 ± 0,0093, $p < 0,0001$°°°° for day 60 *vs.* SP) and decreased immune cell infiltration in the bronchoalveolar fluid (Fig. 3C, 35,00 ± 5580, $p < 0,0001$°°°° for day 42 *vs.* SP; 32,00 ± 3440, $p < 0,0001$°°°° for day 60 *vs.* SP), consistent with the histological staining outcomes. No significant changes in the lung injury score and number of immune cells in the BALF followed the administration of EcN-pAIDA1 in SARS-CoV-2 SP-treated mice, confirming that immunization is strictly related to the expression of SP on the outer membrane of EcN. The measurement of mice body temperature from day 35 to day 60 shows a fever peak at day 39 in the SP-treated group (Figs. 3D, 38,3 ± 0103, $p < 0,0001$**** *vs* Vehicle), which was prevented by EcN-pAIDA1-SP (Fig. 3D, 37,0 ± 0204, $p < 0,0001$°°°° *vs.* SP) but not by EcN-pAIDA1. The intranasal administration of EcN-pAIDA1-SP did not lead to any changes in the lung histology, cell infiltration, and body temperature compared to vehicle mice, confirming its safety used. Together, our results provide evidence of SP-expressing EcN-pAIDA1 effectiveness in the prevention of lung injury caused by SARS-CoV-2 SP through the intranasal route.

3.4. The engineered EcN-pAIDA1-SP prevents the pro-inflammatory response in situ associated with acute and chronic lung damage

The intranasal administration of SP induced an increase in the expression of TLR-4 at both 42 and 60 days (Fig. 4A–B, 0,0177 ± 0,0018, $p < 0,0001$**** for day 42 *vs.* Vehicle; 0,0154 ± 0,00089, $p < 0,0001$**** for day 60 *vs.* Vehicle), with a parallel rise in NLRP3 expression at the same time points (Fig. 4A–C, 0006 ± 0002, $p < 0.0001$**** for day 42 *vs.* Vehicle; 0,0047 ± 0,0014, $p < 0,0001$**** for 60 *vs.* Vehicle). Additionally, a significant infiltration of macrophage into the lung tissue was highlighted by the increased expression of CD68-positive cells at 42 and 60 days (Fig. 4A–D, 0,0065 ± 0,0014, $p < 0,0001$**** for day 42 *vs.* Vehicle; 0,0054 ± 0,00089, $p < 0,0001$**** for day 60 *vs.* Vehicle). The immunization induced by EcN-pAIDA1-SP was effective in preventing the pro-inflammatory response induced by SP administration, with a significant reduction in the expression TLR4 (Fig. 4A–B, 0,0093 ± 0,0014, $p < 0,0001$°°°° for day 42 *vs.* SP; 0,0080 ± 0,0010, $p < 0,0001$°°°° for day 60 *vs.* SP), NLRP3 (Fig. 4A–C, 0,00052 ± 0,00022, $p < 0,0001$°°°° for day 42 *vs.* SP; 0,00038 ± 0,00008, $p <$

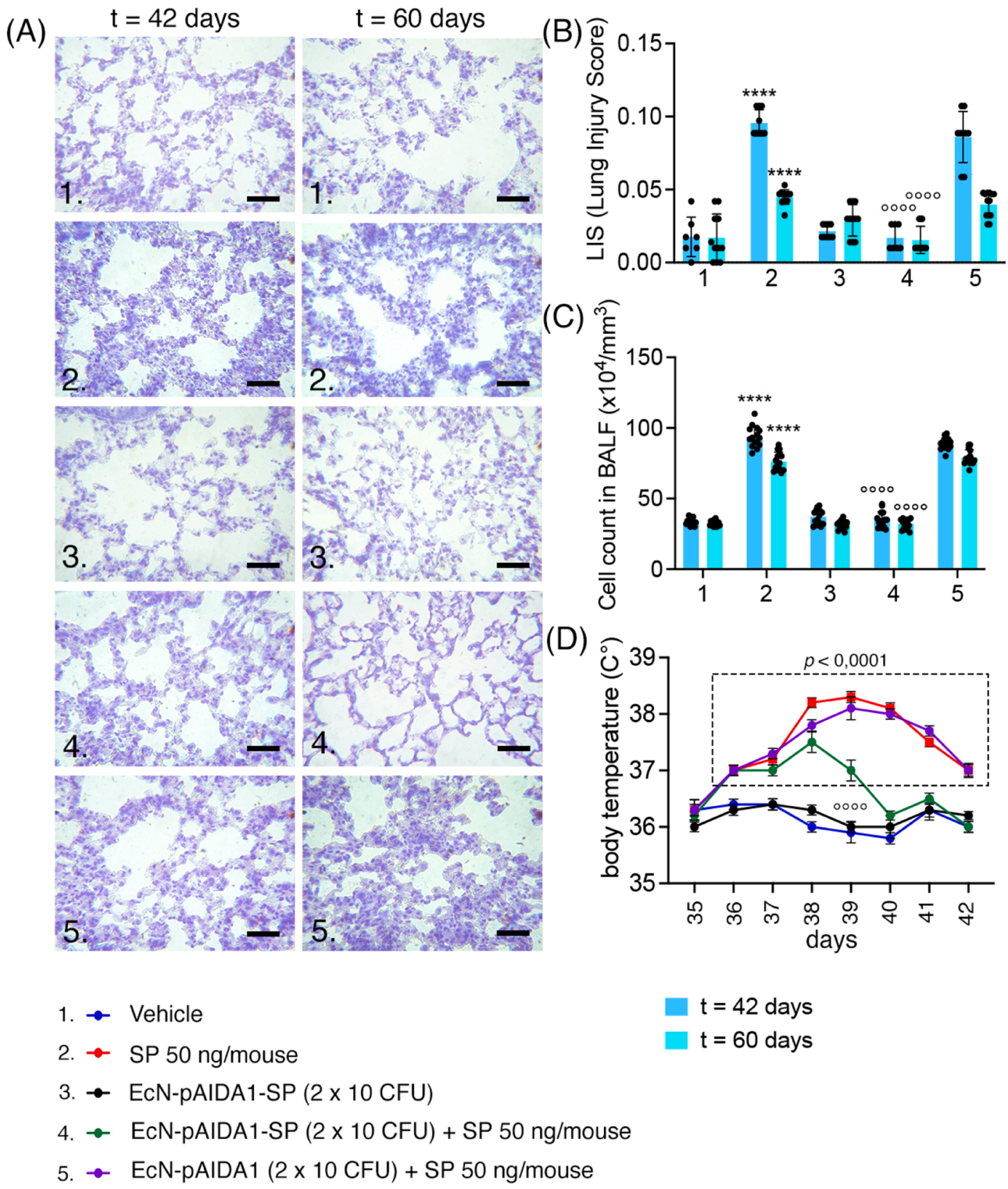

Fig. 3. EcN-pAIDA1-SP prevents SARS-CoV-2 SP-induced lung injury. **(A)** H&E histological staining of lung tissue and related **(B)** the lung injury score is shown at days 42 and 60. **(C)** Cell count in bronchoalveolar fluid and **(D)** measurement of body temperature. Results are presented as the mean ± SD of n = 5 experiments **** $p < 0.0001$ vs. vehicle; oooo $p < 0.0001$ vs. SP. Image magnification 20X.

0,0001°°°° for day 60 *vs.* SP), and CD68 (Fig. 4A–D, 0,0012 ± 0,00066, $p < 0,0001$°°°° for day 42 *vs.* SP; 0,00068 ± 0,00037, $p < 0,0001$°°°° for day 60 *vs.* SP) at 42 and 60 days compared to SP group. The treatment with EcN-pAIDA1 induced similar effects of SARS-CoV-2 SP, confirming that the effectiveness of EcN-pAIDA1-SP was related to the expression of SARS-CoV-2 SP on its outer membrane.

Intranasal administration of SP led to a significantly higher release of pro-inflammatory cytokines, including TNF-α (Fig. 4E, 59,00 ± 3525, $p < 0,0001$**** for day 42 for *vs.* Vehicle; 39,47 ± 3067, $p < 0,0001$**** for day 60 *vs.* Vehicle), IL-1β (Fig. 4F, 10,28 ± 0287, $p < 0,0001$**** for day 42 *vs.* Vehicle; 7612 ± 0251, $p < 0,0001$**** for day 60 *vs.* Vehicle), and myeloperoxidase (MPO) (Figs. 4G, 120, 3 ± 1175, $p < 0,0001$**** for day 42 *vs.* Vehicle; 94,20 ± 2981, $p < 0,0001$**** for day 60 *vs.* Vehicle) compared to the vehicle group at both acute and chronic phase

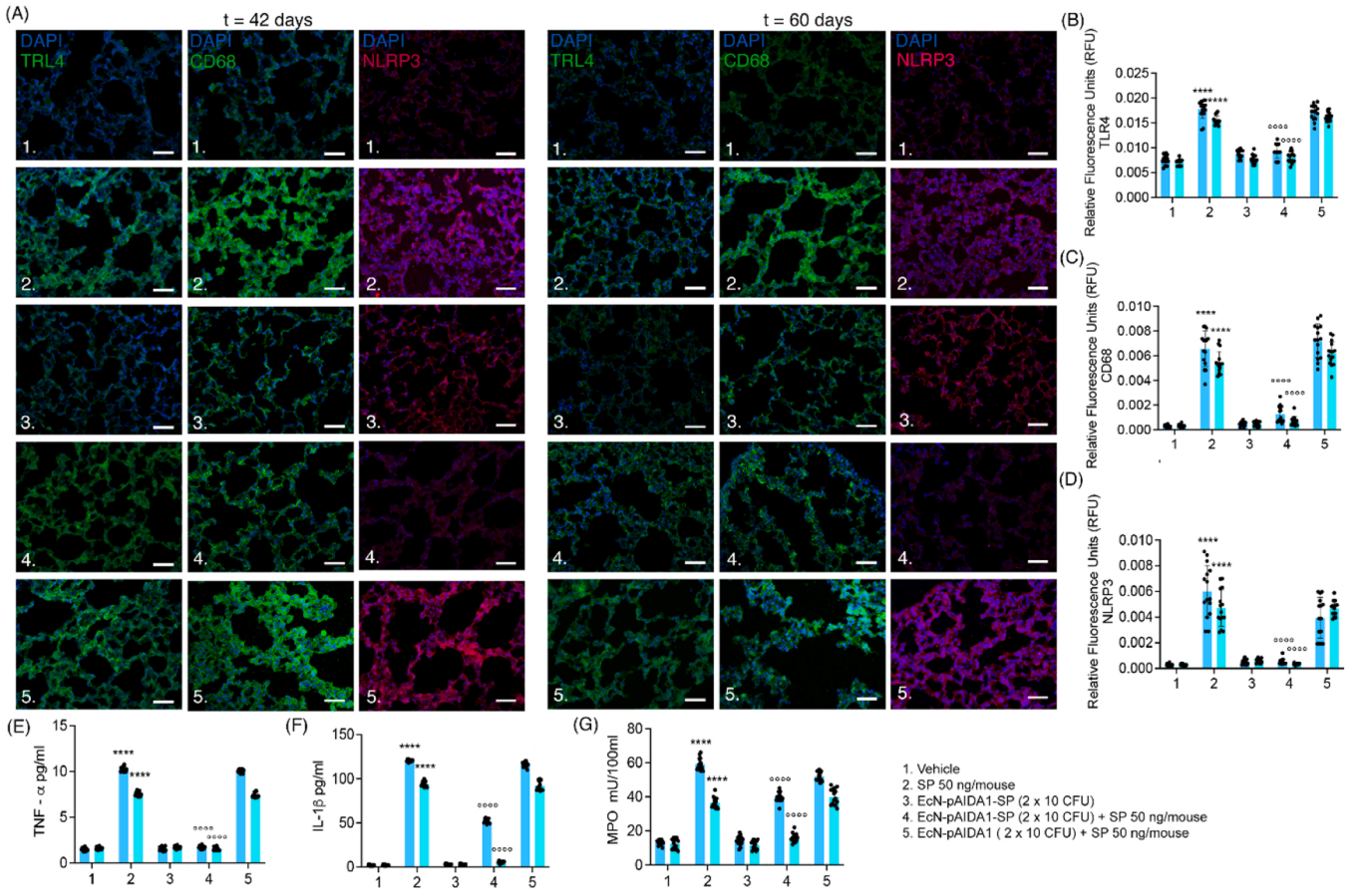

Fig. 4. EcN-AIDA1-SP hinders the upregulation of inflammatory markers, diminishes oxidative stress, and mitigates the release of pro-inflammatory cytokines. In this figure, the expressions of **(A-B)** TLR-4, **(A-C)** CD68, and **(A-D)** NLRP3 are depicted at days 42 and 60, respectively. **(E)** Quantification of TNF-α, **(F)** IL-1β, and **(G)** myeloperoxidase in serum is shown. Results are presented as the mean ± SD of n = 5 experiments **** $p < 0.0001$ vs. vehicle; °°°° $p < 0.0001$ vs. SP; image magnification 20X.

of inflammatory process, respectively. Conversely, the group immunized with EcN-pAIDA1-SP displayed a significant reduction in the release of TNF-α (Figs. 4E, 1,709 ± 0,1598, $p < 0,0001^{°°°°}$ for day 42 *vs.* SP; 1551 ± 0,1856, $p < 0,0001^{°°°°}$ for day 60 *vs.* SP), IL-1β (Fig. 4F, 51,93 ± 2576, $p < 0,0001^{°°°°}$ for day 42 *vs.* SP; 5,4 ± 1121, $p < 0,0001^{°°°°}$ for day 60 *vs.* SP), and MPO (Fig. 4G, 40,07 ± 3025, $p < 0,0001^{°°°°}$ for day 42 *vs.* SP; 16,00 ± 2572, $p < 0,0001^{°°°°}$ for day 60 *vs.* SP), in contrast to the group treated with EcN-pAIDA1. Consistent with the previous results, the intranasal administration of EcN-pAIDA1-SP prevented the lung injury through the inhibition of pro-inflammatory response mediated by SARS-CoV-2 SP.

4. Discussion

Both our research group and other authors have previously advocated for the utilization of probiotic strains as vectors for viral or bacterial antigens, yielding promising results, including efficacy against SARS-CoV-2 as suggested in our previous work [15,45,46]. As the scientific community reflects on the insights gained from the SARS-CoV-2 pandemic, there arise a critical demand for an alternative vaccine platform that is not only cost-effective but also easily scalable, and simpler in terms of storage and administration. This could mitigate the substantial constraints posed by existing COVID-19 vaccines and potentially lay the groundwork for future vaccination strategies against the risk of new pandemic emergencies.

To overcome these limitations, we investigated a probiotic-based immunization administered intranasally, using a genetically modified non-pathogenic EcN strain to express and present the SARS-CoV-2 SP on the bacterial surface. The concept of employing probiotics as a supportive or therapeutic tool in pulmonary conditions is widely embraced, particularly for their anti-inflammatory properties [46–49]. Numerous studies underscore the effectiveness of specific probiotic strains, especially when delivered intranasally, in treating LRT viral infections [50–54].

Intranasal administration of certain strains has demonstrated the ability to modulate the respiratory microbiota composition [52], a key determinant of immune responses [55]. These beneficial microbes reinforce the defense mechanisms of the respiratory tract, promoting a robust and well-balanced immune response to viral infections [56]. By promoting the production of short-chain fatty acids and anti-inflammatory molecules, they have the potential to play a crucial role in quelling the body's inflammatory storm, potentially alleviating the severity of COVID-19 [57]. Intriguingly, specific probiotic strains have displayed direct antiviral effects, showing the ability to inhibit viral replication [47]. Although the precise mechanisms require further exploration, some strains appear to establish an antiviral state in macrophages through the production of nitric oxide (NO) and inflammatory cytokines such as IL-6 and INF-γ. Significantly, probiotic-based vaccines offer solutions to challenges associated with storage and availability. Lyophilization, extending storage time and improving stability, eliminates the need for a cold-supply chain or refrigeration. Moreover, these vaccines do not necessitate specialized personnel or sterile syringes for administration. The feasibility of probiotic-based vaccines establishes them as a practical and realistic solution for addressing the healthcare needs of remote regions and poor nations.

In terms of safety, EcN-pAIDA1-SP effectively colonized the lungs of

mice since day 14th without eliciting a local or systemic pro-inflammatory response following both the initial and booster intra-nasal doses. While there are inherent limitations in using a murine model, such as predicting adverse reactions and translating results to humans, none of the animals in our experiment displayed symptoms related to lung issues or fever. Furthermore, we are confident that EcN-pAIDA1-SP will not exhibit any adverse reactions. This confidence stems from the fact that the chosen antigen carrier, EcN, is a well-established commensal bacterium fully integrated into the human gut microbiota. It possesses immunomodulatory functions that mitigate the inflammatory process [58]. Studies have shown that EcN can induce the production of anti-inflammatory mediators like IL-10, dampening the immune response of T lymphocytes, macrophages, and other immunocompetent cells, even at systemic sites [59,60]. Additionally, EcN stimulates the systemic production of antibodies from B lymphocytes associated with mucous membranes and induces the production of antibodies (IgM, IgA) in adults [61].

In terms of the immune response, the intra-nasal administration of EcN-pAIDA1-SP triggered systemic immunity, as evidenced by detectable anti-SARS-CoV-2 SP IgG in serum samples and IgA in BALF two weeks after the treatment initiation. Following the booster dose, both IgG and IgA levels reached their peak concentrations in the respective samples on the 35th day. Moreover, both serum IgG and secretory IgA exhibited a progressively increased avidity index, indicating selective binding to the SP. While not considered a gold-standard methodology, antibody avidity can be informative in assessing vaccination efficacy. Our results align with a gradually reinforced binding between immunoglobulins and the epitope, reflecting the maturation of the immune response post-booster administration. Additionally, the activation of CD138+ cells in the lungs and spleen serves as direct evidence of long-term immune memory activation since these cells represent the plasmacytic effectors responsible for immunoglobulin production and release. Finally, our findings suggest the potential of EcN-pAIDA1-SP to prevent the invasion and colonization of the intestinal and respiratory mucosa by triggering an IgA-mediated immune response.

To evaluate the neutralizing capacity of post-vaccination antibodies, we administered intranasal doses of the SARS-CoV-2 SP to the animals. The SP of SARS-CoV-2 appears to directly interact with TLR4, triggering a bacteria-like immune response in lung tissue.

Animals treated with SP in our study exhibited increased TLR4 levels in the tissue, along with heightened activation of the NLRP3 inflammasome. At the histological level, we also observed increased pro-inflammatory cells infiltration and disruption of alveolar morphology. Building on prior research, the authors propose that the activation of the TLR4/NF-κB pathway is responsible for initiating the inflammasome protein complex, contributing to the bacteria-like response observed in ARDS patients [31,32].

In our model, the pre-immunized group displayed a reduction in pro-inflammatory markers, coupled with better preservation of tissue morphology. This was attributed to antibodies inhibiting the TLR4/SP interaction, blocking NLRP3 activation, and associated pathways, such as IL-1β. IL-1β is a key mediator in ARDS and is considered a potential target for pharmacological treatment in the early stages of COVID-19. Furthermore, inhibiting the NLRP3/caspase-1 pathway in alveolar macrophages could be crucial in preventing pyroptosis. This inhibition is crucial since, under various pathological conditions, extensive macrophage-induced pyroptosis through NLRP3/caspase-1 activation led to enhanced neutrophil recruitment. The administration of EcN-pAIDA1 did not prevent the effects induced by SARS-CoV-2 SP, confirming that immunization is strictly related to the expression of SP on the outer membrane of EcN. Unlike a mere recombinant production of the Spike protein from bacteria, the membrane anchoring system pAIDA allows for a surface exposure of the recombinant Spike protein to optimize its antigenic potential in terms of immune recognition by the host. Differently by tissue-resident macrophages, neutrophils exhibit heightened immunoreactivity, and their activation can contribute to more severe inflammation. In COVID-19 patients, an over-recruitment of neutrophils during the most severe stage of the disease has been observed.

Therefore, by averting pyroptosis in alveolar macrophages and reducing the release of ILs and other pro-inflammatory mediators, EcN-pAIDA-SP may exert multiple protective effects, preventing the onset of the most severe symptoms in COVID-19 patients.

5. Conclusion

In summary, our study explored the efficacy of the Ecn-pAIDA1-SP probiotic-based vaccine when administered intra-nasally to elicit an immune response against SARS-CoV-2 SP. The safety assessment in mouse models revealed successful colonization of the lungs while preventing pro-inflammatory reactions. Concurrently, we observed activation of antibody-mediated immunity, evidenced by increased CD138+ cell count and production of anti-SP IgG and IgA following administration. The gradual enhancement in antibody avidity further suggests promising immune responses. Additionally, the lungs of the pre-immunized group were shielded from the pro-inflammatory environment following intra-nasal administration of SP from SARS-CoV-2. We also emphasized how probiotic-based vaccines address logistical challenges in terms of storage and accessibility, offering a practical solution for remote regions. The demonstrated preventive capabilities of EcN-pAIDA1-SP against mucosal invasion, coupled with its IgA-mediated immune response, underscore its effectiveness against severe COVID-19 symptoms. The high frequency of sequence mutations (e.g., Omicron B.1.1.529; JN.1, etc.) reported in the Spike protein poses a significant challenge for the new vaccines being proposed against SARS-CoV-2 infections. Although our experimental paradigm has focused, at this stage, on the original variant of the Spike protein, it is not excluded that, through appropriate biotechnological rearrangements, we can display different-antigen expression on bacteria. By this way in the future, it may be possible to induce a probiotic-based poly-immunobiotic capable of expressing multiple antigenic systems of both SARS-CoV-2 and other respiratory viruses.

Patents

Engineering of probiotic *E. coli Nissle 1917* expressing the SARS-CoV-2 spike protein as a chimeric model of intestinal immunization against COVID-19 (wo2022219530 (a1)–2022–10–20).

Institutional review board statement

All in vivo experimental protocols were approved by the animal welfare regulation of University of Naples “Federico II”, Italy, and by the Superior Institute of Health, Italy. Animal studies were carried out in compliance with the ARRIVE (Animal Research: Reporting of In Vivo Experiments) guidelines, E.U. Directive 2010/63/EU for animal experiments.

Funding

This work was supported partially by the PNRR project Rome Technopole to GE (Grant Agreement: ECS00000024; Italian Ministry of University and Education).

CRediT authorship contribution statement

Marcella Pesce: Validation. **Aurora Zilli:** Investigation. **Giovanni Esposito:** Writing – review & editing. **Sara Rurgo:** Writing – review & editing. **Giuseppe Esposito:** Writing – review & editing, Supervision, Project administration, Funding acquisition, Conceptualization. **Giovanni Sarnelli:** Project administration, Conceptualization. **Walter Sanseverino:** Writing – review & editing, Writing – original draft,

Project administration, Methodology, Investigation, Formal analysis, Data curation, Conceptualization. **Irene Palenca:** Writing – original draft, Project administration, Methodology, Investigation, Formal analysis, Data curation, Conceptualization. **Alessandro Del Re:** Writing – review & editing, Writing – original draft, Supervision, Project administration, Methodology, Investigation, Formal analysis, Data curation, Conceptualization. **Jie Lu:** Formal analysis. **Silvia Basili Franzin:** Investigation, Formal analysis. **Seguella Luisa:** Writing – review & editing, Validation, Investigation, Conceptualization.

Declaration of Competing Interest

The authors declare that they have no known competing financial interests or personal relationships that could have appeared to influence the work reported in this paper.

Data Availability

The datasets generated during and/or analyzed during the current study are available from the corresponding authors upon reasonable request. The DNA sequences generated during the current study are available in the AddGene repository.

References

[1] M.M. Lamers, B.L. Haagmans, SARS-CoV-2 pathogenesis, Nat. Rev. Microbiol. 20 (2022) 270–284.
[2] G. Zhang, T. Tang, Y. Chen, X. Huang, T. Liang, mRNA vaccines in disease prevention and treatment, Signal Transduct. Target. Ther. 8 (2023) 1–30.
[3] J.S. Tregoning, K.E. Flight, S.L. Higham, Z. Wang, B.F. Pierce, Progress of the COVID-19 vaccine effort: viruses, vaccines and variants versus efficacy, effectiveness and escape, Nat. Rev. Immunol. 21 (2021) 626–636.
[4] V. Rotshild, B. Hirsh-Raccah, I. Miskin, M. Muszkat, I. Matok, Comparing the clinical efficacy of COVID-19 vaccines: a systematic review and network meta-analysis, Sci. Rep. 11 (2021) 22777.
[5] D.D. Richman, COVID-19 vaccines: implementation, limitations and opportunities, Glob. Health Med. 3 (2021) 1–5.
[6] M. Madhavan, et al., Tolerability and immunogenicity of an intranasally-administered adenovirus-vectored COVID-19 vaccine: An open-label partially-randomised ascending dose phase I trial, eBioMedicine 85 (2022).
[7] A.P.S. Rathore, A.L.S. John, Promises and challenges of mucosal COVID-19 vaccines, Vaccine 41 (2023) 4042.
[8] S.K. Samrat, A.M. Tharappel, Z. Li, H. Li, Prospect of SARS-CoV-2 spike protein: potential role in vaccine and therapeutic development, Virus Res. 288 (2020) 198141.
[9] K. Tan, R. Li, X. Huang, Q. Liu, Outer membrane vesicles: current status and future direction of these novel vaccine adjuvants, Front. Microbiol. 9 (2018).
[10] A. Zariri, P. van der Ley, Biosynthetically engineered lipopolysaccharide as vaccine adjuvant, Expert Rev. Vaccin. 14 (2015) 861–876.
[11] Z.D. Blount, The unexhausted potential of E. coli, eLife 4 (2015).
[12] M. Kamionka, Engineering of therapeutic proteins production in Escherichia coli, Curr. Pharm. Biotechnol. 12 (2011) 268–274.
[13] C.-J. Huang, H. Lin, X. Yang, Industrial production of recombinant therapeutics in Escherichia coli and its recent advancements, J. Ind. Microbiol. Biotechnol. 39 (2012) 383–399.
[14] D.L.N.F. Maeda, et al., Killed whole-genome reduced-bacteria surface-expressed coronavirus fusion peptide vaccines protect against disease in a porcine model, e2025622118, Proc. Natl. Acad. Sci. U. S. A. 118 (2021). e2025622118.
[15] G. Sarnelli, et al., Oral Immunization with Escherichia coli Nissle 1917 expressing SARS-CoV-2 spike protein induces mucosal and systemic antibody responses in mice, Biomolecules 13 (2023) 569.
[16] ChAdOx1 nCoV-19 vaccine prevents SARS-CoV-2 pneumonia in rhesus macaques - PubMed. https://pubmed.ncbi.nlm.nih.gov/32731258/.
[17] K.S. Corbett, et al., SARS-CoV-2 mRNA vaccine design enabled by prototype pathogen preparedness, Nature 586 (2020) 567–571.
[18] L. Liu, et al., High neutralizing antibody titer in intensive care unit patients with COVID-19, Emerg. Microbes Infect. 9 (2020) 1664–1670.
[19] Ziegler, C.G.K. et al. SARS-CoV-2 Receptor ACE2 Is an Interferon-Stimulated Gene in Human Airway Epithelial Cells and Is Detected in Specific Cell Subsets across Tissues. *Cell* **181**, 1016-1035.e19 (2020).
[20] Anti-Spike Mucosal IgA Protection against SARS-CoV-2 Omicron Infection - PubMed. https://pubmed.ncbi.nlm.nih.gov/36103621/.
[21] C.W. Seibert, et al., Recombinant IgA is sufficient to prevent influenza virus transmission in guinea pigs, J. Virol. 87 (2013) 7793–7804.
[22] X. Chen, et al., Macrophage polarization and its role in the pathogenesis of acute lung injury/acute respiratory distress syndrome, Inflamm. Res. 69 (2020) 883–895.
[23] Z. Abassi, Y. Knaney, T. Karram, S.N. Heyman, The lung macrophage in SARS-CoV-2 infection: a friend or a foe? Front. Immunol. 11 (2020) 1312.
[24] B.A. Stanton, T.H. Hampton, A. Ashare, SARS-CoV-2 (COVID-19) and cystic fibrosis, Am. J. Physiol. Lung Cell. Mol. Physiol. 319 (2020) L408–L415.
[25] T. Venkataraman, M.B. Frieman, The role of epidermal growth factor receptor (EGFR) signaling in SARS coronavirus-induced pulmonary fibrosis, Antivir. Res. 143 (2017) 142–150.
[26] T.L. Freeman, T.H. Swartz, Targeting the NLRP3 inflammasome in severe COVID-19, Front. Immunol. 11 (2020).
[27] SARS-CoV-2 drives NLRP3 inflammasome activation in human microglia through spike protein | Molecular Psychiatry. https://www.nature.com/articles/s41380-022-01831-0.
[28] Y. Zhao, et al., SARS-CoV-2 spike protein interacts with and activates TLR41, Cell Res. 31 (2021) 818–820.
[29] S. Sahanic, et al., SARS-CoV-2 activates the TLR4/MyD88 pathway in human macrophages: a possible correlation with strong pro-inflammatory responses in severe COVID-19, Heliyon 9 (2023) e21893.
[30] SARS-CoV-2 Spike protein induces TLR4-mediated long-term cognitive dysfunction recapitulating post-COVID-19 syndrome in mice - PubMed. https://pubmed.ncbi.nlm.nih.gov/36857178/.
[31] A. Del Re, et al., Ultramicronized palmitoylethanolamide inhibits NLRP3 inflammasome expression and pro-inflammatory response activated by SARS-CoV-2 spike protein in cultured murine alveolar macrophages, Metabolites 11 (2021) 592.
[32] C. Corpetti, et al., Cannabidiol inhibits SARS-Cov-2 spike (S) protein-induced cytotoxicity and inflammation through a PPARγ-dependent TLR4/NLRP3/Caspase-1 signaling suppression in Caco-2 cell line, Phytother. Res. PTR 35 (2021) 6893–6903.
[33] V. Hennings, et al., The presence of serum anti-SARS-CoV-2 IgA appears to protect primary health care workers from COVID-19, Eur. J. Immunol. 52 (2022) 800–809.
[34] S. Parasuraman, R. Raveendran, R. Kesavan, Blood sample collection in small laboratory animals, J. Pharmacol. Pharmacother. 1 (2010) 87–93.
[35] E.A. Greenfield, Sampling and preparation of mouse and rat serum, pdb.prot100271, Cold Spring Harb. Protoc. 2017 (2017). pdb.prot100271.
[36] C.W. Meyer, Y. Ootsuka, A.A. Romanovsky, Body temperature measurements for metabolic phenotyping in mice, Front. Physiol. 8 (2017) 520.
[37] P.K.S. Chan, et al., Antibody avidity maturation during severe acute respiratory syndrome–associated coronavirus infection, J. Infect. Dis. 192 (2005) 166–169.
[38] S.E. Benner, et al., SARS-CoV-2 Antibody avidity responses in COVID-19 patients and convalescent plasma donors, J. Infect. Dis. 222 (2020) 1974–1984.
[39] F. Struck, et al., Vaccination versus infection with SARS-CoV-2: Establishment of a high avidity IgG response versus incomplete avidity maturation, J. Med. Virol. 93 (2021) 6765–6777.
[40] L.H. Ling, et al., Comparison of various tissue-preparation techniques for cryosectioning of frozen mouse tissues, J. Histotechnol. 32 (2009) 186–189.
[41] G. Matute-Bello, et al., An Official American Thoracic Society workshop report: features and measurements of experimental acute lung injury in animals, Am. J. Respir. Cell Mol. Biol. 44 (2011) 725–738.
[42] R.K. Paidi, et al., ACE-2-interacting domain of SARS-CoV-2 (AIDS) peptide suppresses inflammation to reduce fever and protect lungs and heart in mice: implications for COVID-19 therapy, J. Neuroimmune Pharmacol. 16 (2021) 59–70.
[43] K.M. Mullane, R. Kraemer, B. Smith, Myeloperoxidase activity as a quantitative assessment of neutrophil infiltration into ischemic myocardium, J. Pharmacol. Methods 14 (1985) 157–167.
[44] J. Domagała-Kulawik, T. Skirecki, M. Maskey-Warzechowska, H. Grubek-Jaworska, R. Chazan, Bronchoalveolar lavage total cell count in interstitial lung diseases–does it matter? Inflammation 35 (2012) 803–809.
[45] E.C.T. Chau, et al., A novel probiotic-based oral vaccine against SARS-CoV-2 omicron variant B.1.1.529, Int. J. Mol. Sci. 24 (2023) 13931.
[46] S. Taghinezhad-S, et al., Probiotic-based vaccines may provide effective protection against COVID-19 acute respiratory disease, Vaccines 9 (2021) 466.
[47] Y. Wang, A. Moon, J. Huang, Y. Sun, H.-J. Qiu, Antiviral effects and underlying mechanisms of probiotics as promising antivirals, Front. Cell. Infect. Microbiol. 12 (2022) 928050.
[48] B. Jiang, Z. Li, B. Ou, Q. Duan, G. Zhu, Targeting ideal oral vaccine vectors based on probiotics: a systematical view, Appl. Microbiol. Biotechnol. 103 (2019) 3941–3953.
[49] C. Mazziotta, M. Tognon, F. Martini, E. Torreggiani, J.C. Rotondo, Probiotics mechanism of action on immune cells and beneficial effects on human health, Cells 12 (2023) 184.
[50] J. Xu, et al., Boosting vaccine-elicited respiratory mucosal and systemic COVID-19 immunity in mice with the oral Lactobacillus plantarum, Front. Nutr. 8 (2021).
[51] I. Spacova, et al., Intranasal administration of probiotic Lactobacillus rhamnosus GG prevents birch pollen-induced allergic asthma in a murine model, Allergy 74 (2019) 100–110.
[52] C.-M. Chen, Y.-C.S.H. Yang, H.-C. Chou, S. Lin, Intranasal administration of Lactobacillus johnsonii attenuates hyperoxia-induced lung injury by modulating gut microbiota in neonatal mice, J. Biomed. Sci. 30 (2023) 57.
[53] H.-N. Youn, et al., Intranasal administration of live Lactobacillus species facilitates protection against influenza virus infection in mice, Antivir. Res. 93 (2012) 138–143.
[54] T.T. Tran, et al., Efficient symptomatic treatment and viral load reduction for children with influenza virus infection by nasal-spraying Bacillus spore probiotics, Sci. Rep. 13 (2023) 14789.
[55] M. Kyo, et al., Unique patterns of lower respiratory tract microbiota are associated with inflammation and hospital mortality in acute respiratory distress syndrome, Respir. Res. 20 (2019) 246.

[56] R. Li, J. Li, X. Zhou, Lung microbiome: new insights into the pathogenesis of respiratory diseases, Signal Transduct. Target. Ther. 9 (2024) 1–27.
[57] J. Włodarczyk, B. Czerwiński, J. Fichna, Short-chain fatty acids–microbiota crosstalk in the coronavirus disease (COVID-19), Pharmacol. Rep. 74 (2022) 1198–1207.
[58] Helmy, Y.A., Kassem, I.I. & Rajashekara, G. Immuno-modulatory effect of probiotic E. coli Nissle 1917 in polarized human colonic cells against Campylobacter jejuni infection. *Gut Microbes* **13**, 1857514.
[59] A. Sturm, et al., Escherichia coli Nissle 1917 distinctively modulates T-cell cycling and expansion via toll-like receptor 2 signaling, Infect. Immun. 73 (2005) 1452–1465.
[60] Anti-inflammatory modulation of immune response by probiotic Escherichia coli Nissle 1917 in human blood mononuclear cells - Anne-Katrin Güttsches, Stefan Löseke, Ulrich Zähringer, Ulrich Sonnenborn, Corinne Enders, Sören Gatermann, Albrecht Bufe, 2012. https://journals.sagepub.com/doi/10.1177/1753425910396251.
[61] A.M. Westendorf, et al., Intestinal immunity of Escherichia coli NISSLE 1917: a safe carrier for therapeutic molecules, FEMS Immunol. Med. Microbiol. 43 (2005) 373–384.